American Mineralogist, Volume 93, pages 414–425, 2008

The octahedral sheet of metamorphic $2M_1$-phengites: A combined EMPA and AXANES study

Giannantonio Cibin,[1,2,*] Gianfelice Cinque,[2,3] Augusto Marcelli,[2] Annibale Mottana,[1,2,†] and Raffaele Sassi[4]

[1]Dipartimento di Scienze Geologiche, Università degli Studi Roma Tre, Largo San Leonardo Murialdo 1, 00146 Roma, Italy
[2]Laboratori Nazionali di Frascati, Istituto Nazionale di Fisica Nucleare, Via Enrico Fermi 40, 00030 Frascati RM, Italy
[3]Diamond Light Source, Rutherford Appleton Laboratory, Chilton, Didcot, Oxfordshire OX11 0QX, U.K.
[4]Dipartimento di Mineralogia e Petrologia, Università degli Studi di Padova, Corso Giuseppe Garibaldi 37, 35122 Padova, Italy

Abstract

Two types of metamorphic phengites are known: one is linked to high pressure and is $3T$; the other is $2M_1$, and its composition is linked to rock-compositional constraints. This work investigates the octahedral sheet crystal-chemical differences between the two phengite types. Seven dioctahedral micas were studied: (1) one $3T$ phengite from an ultrahigh-pressure metagranitoid in the Dora Maira massif, Italy ($P \sim 4.3$ GPa, $T \sim 730$ °C); (2) five $2M_1$ phengites from medium-P orthogneisses in the Eastern Alps metamorphic basement, Italy ($P \leq 0.7$ GPa, $T \sim 500$–600 °C); and (3) one $2M_1$ ferroan muscovite from pegmatite in Antarctica ($P \leq 0.2$ GPa, $T \sim 500$ °C). All micas display significant extents of celadonite substitution. In particular, the $2M_1$-phengite formulae (calculated on the basis of 11 O) have $0.68 < {}^{IV}Al < 0.82$ atoms per formula unit (apfu); octahedral atoms are dominated by Al (1.6–1.8 apfu), with minor and variable Fe (0.20–0.35 apfu) and Mg (0.05–0.17 apfu), and very minor Ti, Mn, and Cr. Total octahedral occupancies are slightly above 2.00 apfu, i.e., there seems to be partial occupancy of the third M site. For all micas, we recorded XAFS spectra on mosaics of carefully separated flakes oriented flat on a plastic support that could be rotated so as to account for the polarization of the synchrotron radiation beam, and we processed them on the basis of the AXANES theory. Spectra show angle-dependent absorption variations for Al and Fe, which can be deconvoluted and fitted by dichroic effects. Pre-edges consistently show most Fe to be Fe^{3+} and little angle-dependent intensity variations. The $2M_1$-ferroan muscovite from Antarctica displays the same AXANES behavior as $2M_1$-phengites. By contrast, the ultrahigh-pressure $3T$-phengite from Dora Maira (having ${}^{IV}Al = 0.42$ apfu, and Al and Mg as the dominant octahedral constituents) has XAFS spectra that differ significantly. Not only is the ${}^{IV}Al$ feature strongly reduced, in agreement with the increased Si content, but also Fe XAFS spectra show one broad feature only, indicating that all Fe is Fe^{2+} in a fully disordered distribution with no angle-dependent variations. We conclude that this $3T$-phengite is actually contaminated by exsolved Fe-bearing pyrope platelets, which cannot be resolved under SEM examination; by contrast, the $2M_1$-phengites, unrelated to high-pressure, suggest Al/Fe^{3+} order over the M1 and (M2, M3) sites, as also does the $2M_1$ pegmatitic muscovite.

Keywords: Muscovite, aluminoceladonite, celadonite, white micas, dioctahedral micas, XAFS, XANES, geothermobarometry

Introduction

The I.M.A. nomenclature of micas defines phengite as a series name designating the "potassic dioctahedral micas between, or close to, the joins muscovite-aluminoceladonite and muscovite-celadonite" (Rieder et al. 1998, p. 583, their Table 4). Such a definition is a compromise seeking consensus for the two types of phengites that are usually referred to in the minerologic-petrographic literature: (1) white micas with Si in excess of 3 apfu in the tetrahedral T site, thus lying on the joins muscovite, KAl_2 $KAl_2\square[AlSi_3O_{10}(OH)_2]$, -aluminoceladonite, $KAl(Mg,Fe^{2+})\square[Si_4O_{10}(OH)_2]$, viz. ferro-aluminoceladonite, $KAl(Fe^{2+},Mg)\square[Si_4O_{10}(OH)_2]$, and muscovite-celadonite, $KFe^{3+}(Mg,Fe^{2+})\square[Si_4O_{10}(OH)_2]$, viz. ferroceladonite, $KFe^{3+}(Fe^{2+},Mg)\square[Si_4O_{10}(OH)_2]$; (2) white micas with fairly large amounts of Mg and Fe (whatever its oxidation state) and other scarce heavy cations such as Ti, Cr, etc. in the octahedral M site, the name thus meaning any mica with variable amounts of octahedral Al substituted mostly by Mg and Fe, irrespective of whether it is tetrasilicic or not, but implicitly assuming charge balance. Moreover, the I.M.A. tries to define more exactly phengites on the basis of exchange vectors and cation ratios (Rieder et al. 1998, their Figs. 1a and 1b), and Tischendorf et al. (2004) worked out a bi-dimensional plot

* Current address: Diamond Light Source, Rutherford Appleton Laboratory, Chilton, Didcot, Oxfordshire OX11 0QX, U.K.
† E-mail: mottana@uniroma3.it

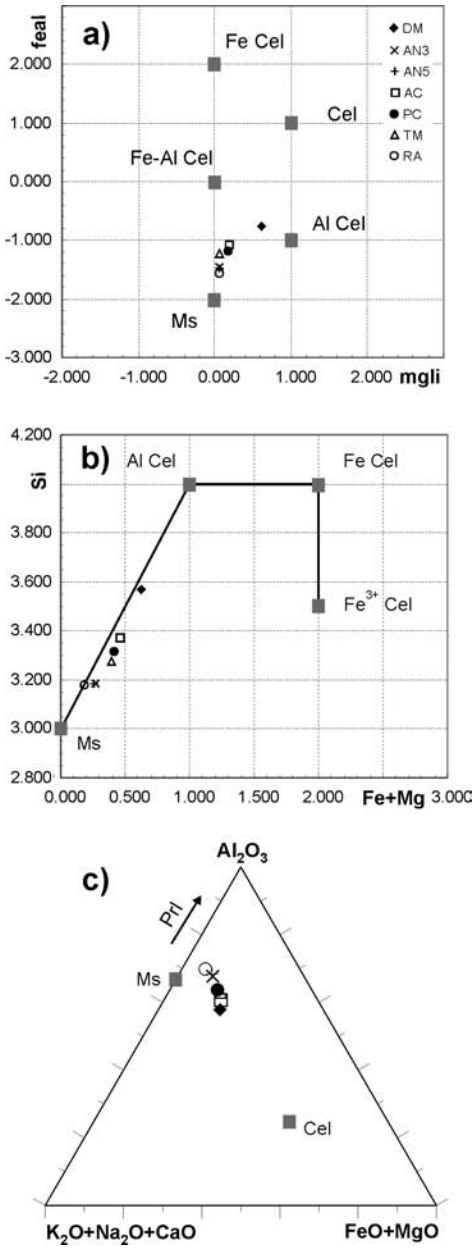

Figure 1. Main chemical features of the studied potassic white micas. (**a**) and (**b**) after Tischendorf et al. (2004): **mgli** = (Mg – Li); **feal** = (Fe_{tot} + Mn + Ti – ^{VI}Al); (**c**) correlation of Si (apfu) vs. the extent of the deviation of the phengite data points from the muscovite (Ms)-celadonite (Cel) tie line. Key for symbols on top of Table 1.

(their Fig. 5) that fits such deeds enough. However, the actual full extent of the phengite space is still a matter of debate, so that an empirical, but widely circulating ideal formula for phengite is $K(Al_{1.5}Mg_{0.5})[(Si_{3.5}Al_{0.5})O_{10}(OH)_2]$ (e.g., Pavese et al. 2003). The matter is complicated further by the fact that, in metamorphic rocks, there are at least two types of white micas showing different stacking sequences; they are the 3*T*-(space group $P3_112$) and $2M_1$-phengites (space group *C*2/*c*). The two polytypes may coexist in the same hand specimen and even in the same flake, despite showing significant chemical zoning and even structural differences (e.g., Ivaldi et al. 2001).

The Si content determined by EMPA in dioctahedral micas rarely exceeds the value 3.61 apfu for 3*T*-phengites (e.g., Amisano-Canesi et al. 1994; Ferraris et al. 2005), and is 3.39 apfu for a vein $2M_1$-phengite (Güven 1971). As a matter of fact, higher values for $2M_1$-mica phases have been determined, but these micas are usually classified as celadonite rather than phengite (Tischendorf et al. 2004, their Figs. 5 and 6). The highest total value for total octahedral occupancy (^{VI}R) rarely exceeds 2.00 apfu (Guidotti and Sassi 1998a, 1998b) and is essentially independent of the stacking type. Indeed, in the graphical compilation of Tischendorf et al. (2004), most dioctahedral micas show $^{VI}R \leq 2.00$, but quite a few of them have $^{VI}R \geq 2.00$ (Fig. 5), so that a clear-cut separation between the phengite and celadonite fields was proposed (Tischendorf et al. 2004, their Fig. 8), which in terms of atoms is at a (Mg + Fe_{tot}) content slightly over 1.00 apfu (Fig. 6). The small excess octahedral occupancy has been quantified to be 0.01–0.05 apfu (Guidotti and Sassi 1998a, Table 3.1) i.e., very small, but statistically significant. Thus, many chemical substitutions are involved in the structural and charge-equilibration processes by which the tetrahedral (T) and octahedral (O) sheets of phengites change their sizes so as to match structurally (Guidotti and Sassi 1998b, p. 61). Theoretically, the two substitutions should balance and, in particular, they are strictly obliged to maintain a ratio that accounts for the dioctahedral structure (M = 2) emblematic of all white micas. However, in the real world, many phengites do not equilibrate compositionally, either for the excess charge in the T sheet induced by the Si > 3 apfu value is greater than the charge defect determined in the O sheet even after reducing some Fe^{3+} to Fe^{2+}, or because there is still an excess of total M cations after such a reduction. This is the basic reason for the suggestion that there is indeed a partial occupancy of the third octahedral site ($2 \leq M \leq 3$) i.e., the site that is vacant in ideal dioctahedral micas (Guidotti 1984, p. 373; Guidotti and Sassi 1998a, p. 824; Guidotti and Sassi 2002, p. 417), although to a very limited extent (<10%).

Dioctahedral micas are a useful and reliable tool for deriving metamorphic *P*-*T* conditions, when appropriately used. However, misfit between the T vs. O sheet compositional ratios would strongly reduce the reliability of methods based on cation exchange (Massonne and Schreyer 1987; Guidotti and Sassi 1998a, 1998b). In particular, determination of cation ordering, either between Al and Si in the T sheet, or between Al, Mg, and Fe in the O sheet, is strongly hindered. Knowing order-disorder (O-D) relationships helps significantly in establishing enthalpy calculations on firm grounds (McConnell et al. 1997), and these calculations, in turn, are desirable for they have been shown to change petrological predictions significantly (Massonne 1995; Vieillard 1995).

To conclude, phengites have shown to be extremely promising to assess *P*-*T* conditions, particularly for metamorphic series spanning very low to high thermal regimes (cf. Guidotti and Sassi 2002, and references therein; cf. also Ferraris et al. 2005; Kisch et al. 2006) and, as such, they partake in several geothermobarometric methods commonly in use (cf. Spear 1993, and references therein). Consequently, a new attempt at determining their main atom O-D distributions in the T and O sheets appears

to be useful. Such a new attempt should use methods different from, and additional to the already well-established ones, such as single-crystal XRD (e.g., Amisano-Canesi et al. 1994; Smyth et al. 2000), powder ND (e.g., Pavese et al. 1997, 1999a, 2001; Mookherjee et al. 2001), and powder XRD with full-profile Rietveld data treatment (Pavese et al. 1999b; Schmidt et al. 2001). Note, moreover, that to the aim of determining ordering in phengites, indirect methods such as computational studies have also been attempted (Palin et al. 2003); their results suggest that it is necessary to try alternative ways that would support their predictions better. The new method cannot be other than one based on spectroscopy, because this type of material analysis has rarely been applied to micas, less than others on phengites, but it has shown its potentials for a variety of mineral groups (e.g., NMR: Sanz 1988; IR: Beran 2002; Optics and ME: Dyar 2002; and references listed in them).

The spectroscopic method we plan to apply is X-ray absorption fine-structure spectroscopy (XAFS) (Mottana et al. 2002; Mottana 2004) in the modification named angle-dependent X-ray absorption near-edge structure spectroscopy (AXANES) (Brouder et al. 1990). XAFS is well-known to be a very local probe that is chemically specific, highly resolved in space and time, and able to detect minor to trace amounts particularly of the heavy atoms. Furthermore, synchrotron radiation (SR) is strongly linearly polarized (>90%), so that angle-dependent absorption spectra appear to be quite fit for the mica platy morphology and structure. Indeed, they have been commonly applied to clays (as well as, rarely, to micas), albeit mostly in the relatively simple experimental set up satisfying the requirements for data treatment by the extended X-ray absorption fine structure (EXAFS) theory (e.g., Bonnin et al. 1985; Manceau 1990; Manceau et al. 1988, 1990, 1998, 1999, 2000; Manceau and Schlegel 2001). Evidence for polarization dependence is plenty also for the XANES region (e.g., Kutzler et al. 1981; cf. for micas: Dyar et al. 2002a; Mottana et al. 2002; Tombolini et al. 2002). However, the AXANES treatment, despite of having a solid theoretical basis (Izraileva 1966, 1969; Brouder 1990), has been rarely applied to any mineral, mainly because it implies a great number of experiments, long sitting times at SR sources, and time-consuming mathematical fitting of the data. We made use of it only recently for trioctahedral micas at the K *K*-edge and achieved satisfactory results (Cibin et al. 2006; Marcelli et al. 2006). Thus, we are going to test again its ability here and will analyze the Al and Fe *K*-edges that are appropriate for the phengite problem. Conversely, and consequently, we were forced to study a small sample set, which is nevertheless adequate as reference for future petrological applications of XAFS, as it refers to typical, well-known case studies.

Materials

All $2M_1$-phengites are from the Austroalpine Basement of the Eastern Alps (Italy); four (AN3, AN5, AC6, PC7) were from its eastern sector, and one (TM6) from the western sector, as defined in Sassi et al. (2004; cf. their Figs. 2 and 3). The phengitic composition of these dioctahedral K-micas appears to be unrelated to high-*P* conditions; rather, it seems to reflect rock-bulk compositional features, namely low Al content with reference to the Al_2O_3-Na_2O-K_2O plot in the system SiO_2-Al_2O_3-Na_2O-K_2O-H_2O. Thus, they are "type II" phengites as defined by Sassi et al. (1994).

Samples AN3 and AN5 were extracted from two rock samples that are located at a distance of about 150 m one to the other, both belonging to a body known as the "Anterselva orthogneiss" i.e., a former granite to granodiorite body changed into Kfs-bearing orthogneiss by the Variscan metamorphism. The outcrops are in the Anterselva (Antholz) valley close to Bagni di Salomone (Salomonsbrunn). The metamorphic conditions are estimated to be T ~550–600 °C; $P \leq 0.6$ GPa (Spiess et al. 2001).

Samples AC6 and PC7 were extracted from two outcrops in the Riva (Rain) valley about 200 m apart, in between Acereto (Ahornach) village and the Campo Tures (Sand in Taufers) stadium. The rocks are Kfs-bearing augen gneisses making up a thick and large sheet-like body, which derived from felsic volcanic rocks of Upper Ordovician age that is known as "Campo Tures Augengneiss." The main metamorphism is Variscan, related to medium-*P* amphibolite-facies conditions (T ~500–550 °C, $P \leq$ 0.6 GPa), but the rocks underwent also a medium-*P* greenschist-facies overprint of Alpine age.

Phengite TM6 was extracted from a Kfs-bearing orthogneiss known as "Tumulo orthogneiss" collected on the southern slope of Mount Croda Nera (Schwarze Wand) in upper Tumulo (Timmel) valley. This rock unit occurs in the western section of the Austroalpine Basement, close to the boundary between Austria and Italy. It represents Upper Ordovician granitoids changed into Kfs-bearing orthogneisses during low- to medium-*P* Variscan metamorphism, and underwent a greenschist-facies Alpine overprint, to which a *P* value of about 0.7 GPa may be referred. More details about chemistry, geochronology, lithostratigraphic position, and metamorphism of all the orthogneisses containing the above phengites may be found in Mazzoli et al. (2000) and Sassi et al. (2004), and in the references quoted therein.

For comparison, we examined a $3T$-phengite from a metagranitoid in the Brossasco-Isasca unit of the Dora Maira massif (western Alps). This rock, also known as whiteschist because of its white sheen (Schertl et al. 1991), was metamorphosed at ca. 35 Ma (Gebauer et al. 1997) under maximum ultrahigh-pressure conditions (ca. 730 °C and 4.3 GPa; Nowlan et al. 2000; Hermann 2003), but it underwent a multistage decompression path that could go as far as to form thin $2M_1$-phengite rims around the coarse $3T$ grains (Compagnoni and Rolfo 2003; Ferraris et al. 2005).

For further comparison, we also studied a ferroan $2M_1$-muscovite from an Antarctic pegmatite (RA1) of unknown age, crystallized at medium-*T* (ca. 500 °C) and low-*P* (ca. 0.2 GPa) and yet containing Si in slight excess over 3 apfu in the T sheet, combined with significant amounts of Fe and Mg in the O sheet (Brigatti et al. 1998).

The last two white micas had been fully characterized previously from the crystal-chemical and structural viewpoints (Amisano-Canesi et al. 1994; Pavese et al. 1997, 1999b; Brigatti et al. 1998). The data on phengites from the Eastern Alps are new. These phengites were studied from the microchemical point of view (EMPA) and for polytype determination by means of powder X-ray diffraction (P-XRD). Sample provenance, rock assemblage data, and representative chemical analyses are given in Table 1.

Analytical methods

EMPA

The phengites from the Eastern Alps and from Dora Maira were analyzed using a Cameca Camebax electron microprobe (IGG-CNR—Department of Mineralogy and Petrology, University of Padua). Operating conditions were electron beam current 10 nA; accelerating voltage 15 kV; acquisition time 10 s for each element and 5 s on background; beam radius 1 μm. These conditions were established after a rigorous set of experiments on natural dioctahedral K-micas aimed at finding the best EMPA condition to avoid beam-induced alkali loss. Natural and synthetic standards were used, and the PAP correction procedure was followed. Analytical measurements are affected by a relative uncertainty of 1% for the major elements (>5 wt%) and ca. 4% for the minor elements (<5 wt%). All grains submitted for XAFS analysis are unzoned and homogeneous in composition, with the numerous point analyses performed never exceeding the above uncertainty limits. The ferroan muscovite from Antarctica was analyzed using an ARL-SEMQ at Modena University probe for major elements, including F, added with the weight loss determined by thermal analysis using a Seiko SSC 5200 instrument at Modena University and corrected for the microchemical determination of Fe oxidation states (cf. Brigatti et al. 1998). Chemical formulae have been computed on the basis of O = 11 apfu, as usual with micas where no independent determination of volatile content and oxidation state are available.

XAFS

XAFS measurements were carried out both at Stanford Synchrotron Radiation Laboratory (SSRL) and at Laboratori Nazionali di Frascati (LNF) of Istituto Nazionale di Fisica Nucleare (INFN).

At SSRL Al *K*-edge spectra were recorded at beam line SB03-3, the radiation source being SPEAR2 (the now disassembled storage ring) operating at 3 GeV with current decreasing from 90 to 60 mA. The JUMBO monochromator was equipped with an YB_{66} crystal cut along the 004 plane, giving a resolution better than 0.55 eV (Rowen et al. 1993). Mica blades ca. 10 × 5 × 0.3 mm in size were fastened flat onto a vertical Ag-coated sample holder, which could be rotated up to a maximum θ ~75° from the impinging horizontally polarized synchrotron radiation beam. Spectra were recorded at room temperature (RT) with 0.5 eV steps for 6–8 s. A few Fe *K*-edge spectra were recorded at beam line SB04-1 equipped with an Si(111) double-crystal giving a resolution of ca. 1.5 eV (Tombolini et al. 2002), in the fluorescence mode and in air, using a Lytle detector with Soller slits and with the sample compartment filled with N_2 (Lytle et al. 1984). However, most Fe *K*-edge spectra of phengites were recorded at beam line 2–3, with SPEAR3 (the newly installed radiation source) operating at ca. 100–80 mA, in the fluorescence mode using a 13-element Ge detector at resolution ca. 1.2 eV. The polarized spectra were acquired by rotating the sample holder around its vertical axis at angles increasing from 0 to 85°, and the mica blade mosaics were oriented with their *c** axis lying in the horizontal plane.

At LNF, the experiments were carried out at DAΦNE, the storage ring used parasitically for synchrotron radiation research. Its unique characteristics of low energy (0.51 GeV) combined with high current (up to ca. 2 A) provide an intense photon emission peaked in the low-energy range (Burattini et al. 2004). The soft X-ray beam line, DXR-1, is endowed with a Toyama double-crystal fixed-exit monochromator working in "boomerang" geometry with Bragg's angles from 15 to 75°. Aluminum *K*-edge spectra were recorded using Ge(111) crystals for a final energy resolution better than 0.7 eV. A carefully organized mosaic of 0.5 × 0.5 mm wide and 0.02 mm thick mica blades deposited on Kapton tape was loaded in the 8 × 4 mm experimental chamber where the sample holder could be rotated from 0 to 70° from the impinging horizontally polarized synchrotron radiation beam. Spectra were recorded under high vacuum at RT in the transmission mode, at steps ranging from 0.2 to 0.5 eV, using two identical 19 cm long ionization chambers filled with Ar or N_2 gas.

At both facilities and for both atoms, all *K*-edge spectra were recorded sequentially by applying 15° rotations, and often repeated so as to test the accuracy of the results with the SR source decreasing energy.

Table 1. Geographical locations, geological and petrological settings, electron microprobe analyses, and structural data of the studied white micas

Sample no.	DM	AN3	AN5	AC6	PC7	MT7	RA1
Locality	Dora Maira	Valle di Anterselva	Valle di Anterselva	Acereto	Campo Tures	Valle del Tumulo	Antarctica
Rock	metagranitoid	orthogneiss	orthogneiss	orthogneiss	orthogneiss	orthogneiss	pegmatite
Assemblage	Qtz, Ky, Phe, Gnt, Rt	Pl, Kfs, Phe, Qtz, Bt, Chl, Ap	Pl, Kfs, Qtz, Phe, Bt, Chl, Ap, Zrn	Pl, Kfs, Qtz, Phe, Bt, Ep, Chl, Ap, Zrn	Pl, Kfs, Qtz, Phe, Bt, Chl, Ap, Ep	Pl, Qtz, Phe, Kfs, Bt, Chl, Gnt, Ap	single crystal
Chemical composition (wt% oxide)							
SiO_2	54.21	46.55	46.72	47.43	48.19	46.66	47.45
TiO_2	0.35	0.33	0.37	0.32	0.35	0.79	0.79
Al_2O_3	23.55	31.76	32.04	29.00	28.19	31.94	32.98
Cr_2O_3	0.02	0.01	0.04	0.01	0.01	0.03	–
FeO	0.12	3.61	3.29	5.57	4.19	3.40	2.18
MnO	0.00	0.08	0.06	0.12	0.02	0.07	0.05
MgO	6.29	0.59	0.67	0.66	1.65	0.64	0.65
CaO	0.01	0.01	0.00	0.01	0.01	0.00	0.00
Na_2O	0.15	0.36	0.41	0.24	0.21	0.39	0.66
K_2O	10.59	10.56	10.42	10.70	10.69	10.47	10.74
Sum	95.29	93.86	94.02	94.06	93.52	93.96	95.55
Formula proportions (apfu) based on O = 11.000							
Si	3.571	3.184	3.182	3.273	3.318	3.182	3.178
^{IV}Al	0.429	0.816	0.818	0.727	0.682	0.818	0.822
Sum T	4.000	4.000	4.000	4.000	4.000	4.000	4.000
^{VI}Al	1.399	1.745	1.753	1.631	1.605	1.750	1.778
Cr	0.001	0.001	0.002	0.000	0.001	0.002	–
Ti	0.017	0.017	0.019	0.017	0.018	0.018	0.040
Fe^{2+}	0.007	0.206	0.188	0.322	0.241	0.194	0.122
Mn	0.000	0.005	0.004	0.007	0.001	0.004	0.005
Mg	0.618	0.060	0.068	0.068	0.170	0.065	0.056
Sum M	2.042	2.033	2.033	2.044	2.036	2.033	2.001
Ca	0.001	0.001	0.000	0.001	0.000	0.000	–
Na	0.020	0.047	0.054	0.032	0.028	0.052	0.089
K	0.890	0.922	0.905	0.942	0.939	0.911	0.918
Sum A	0.910	0.970	0.959	0.974	0.967	0.963	1.007
X-ray diffraction data							
Polytype	3*T*	$2M_1$	$2M_1$	$2M_1$	$2M_1$	$2M_1$	$2M_1$
d_{002} (Å)		4.9779(3)	4.9815(5)	4.9687(5)	4.9735(4)	4.9753(4)	
b_0 (Å)		9.0361(4)	9.0350(3)	9.0477(4)	9.0449(4)	9.0496(3)	

Notes: – means not determined or below detection limit. RA1 analysis includes: H_2O 4.14 (OH^- 1.851), F 0.35 (F^- 0.073), Sum 99.99 (Brigatti et al. 1998, p. 778). Crystal structure refinement data: Dora Maira phengite: a = 5.215(1) Å, c = 29.755(5) Å, β = 120°, V = 700.8(2) Å^3 (Amisano-Canesi et al. 1994, p. 491); Antarctica RA1 ferroan muscovite: a = 5.182(3) Å, b = 8.982(5) Å, c = 20.002(5) Å, β = 95.72(2)°, V = 926.4(5) Å^3 (Brigatti et al. 1998, p. 776).

Spectrum analysis

Data reduction was been carried out according to the classical procedure described elsewhere (cf. Mottana 2004); in the order: (1) energy calibration; (2) spectrum normalization at ca. 50 eV above threshold; and (3) edge position tracking and extraction of the fine structures via fitting the minima in the derivative patterns. In particular, pre-edges were extracted after subtraction of an arctangent fitting of the XANES tail at the high energy and quantitatively evaluated by fitting pseudo-Voigt functions. Structures are accurate to ±0.3 eV near the absorption *K*-edge, and up to ±1 eV at higher energy; intensities (in arbitrary units relative to a height of 1.0 assumed for the energy of normalization) were found to be reproducible to ±2% relative in duplicate tests. Local behavior and ordering configuration have been studied in the theoretical framework of the multiple-scattering (MS) theory (Natoli et al. 2003; cf. Mottana 2004). Formerly, this was usually done using randomly oriented powders (Mottana et al. 2002); here, we expand the analysis by using single crystals or oriented mosaics and by taking advantage of the angular dependence of XAFS, according to the AXANES theory conceived by Izraileva (1966, 1969) and implemented by Brouder (1990). We follow experimental and mathematical treatments described elsewhere for the K *K*-edge angle-dependence of trioctahedral micas (Cibin et al. 2006; Marcelli et al. 2006), using an algorithm that extrapolates them to any θ rotation angle; in particular, to θ = 0° (σ_{ν}), 90° ($\sigma_{\perp}$) and 35°26 (θ_m).

Results

Mineral chemistry

Table 1 shows the chemical data obtained for all micas. It is worth noting that Si is always significantly higher than 3.0 apfu but varies widely (3.57–3.18 apfu). The variation range of the parameter *RM* (*RM* = ½Fe_2O_3 + FeO + MgO, all in molecular proportions) is smaller (0.047–0.158), as are the sums of octahedral M cations (2.03–2.04). They both fall nicely in the ranges indicated by Guidotti and Sassi (1998a) as typical for phengites. Our EMP analysis of the DM phengite agrees well with that reported by Amisano-Canesi et al. (1994, their Table 1), thus justifying our decision to use their single-crystal XRD data to interpret our AXANES results.

Figure 1 shows the main isomorphous substitutions that dominate the mineral chemistry of potassic micas (Tischendorf et al. 2004). They pointed out that the aluminoceladonite substitution is the most relevant factor in our mica chemical system. As expected, the highest phengite content is found in the ultrahigh-pressure mica of the Dora Maira massif (Figs. 1a and 1b). The phengite contents found in the Eastern Alps samples fall in the same range as dioctahedral K-micas from high-pressure terrains do, although the orthogneisses containing them are unrelated to high-pressure conditions: consequently, their phengitic composition is due to peculiar bulk-chemical constraints at *P-T* conditions under which dioctahedral K-mica usually takes on the composition of muscovite in pelitic systems.

Since our EMPA procedure excludes possible artifacts, the deviation of our phengite data points from the Ms-Cel tie line (Fig. 1c) is consistent with the A cation deficiency detected in their interlayer site (0.09–0.03 apfu: Table 1). Such a deficiency may be due to several reasons (Guidotti and Sassi 1998a, 1998b) including, possibly, the pyrophyllite (Prl) substitution (e.g., Rimmelé et al. 2005). It is worth noting that the extent of the above-mentioned deviations show a good negative correlation with Si contents.

The Antarctic muscovite chemical system differs somewhat from the Eastern Alps phengite one: there is neither alkali deficiency nor excess cations in the O sheet, but only a small excess of Si in the T sheet. Indeed, this ferroan mica cannot be equated to phengite: it is a muscovite, where the excess charge (0.178) of the T sheet due to Si > 3 is almost exactly compensated by the sum of the cations Fe, Mg, and Mn located in the O sheet.

Polytypism

Consistent with the results of Sassi et al. (1994) for "type II" phengite, all our five Eastern Alps phengites unrelated to high-pressure conditions display the $2M_1$ polytype. This is also the case of the pegmatite muscovite from Antarctica (Brigatti et al. 1998). Their powder-XRD spectra show diagnostic lines that fit well with those given by Bailey (1984) and Drits and Sakharov (2004) for polytype $2M_1$, whereas those diagnostic of the 3*T* stacking sequence are lacking. By contrast, only these lines indicative of the 3*T* polytype occur in the ultrahigh-pressure DM phengite powder-XRD spectra. Therefore, in agreement with Sassi et al. (1994), in our data set, only dioctahedral K-micas related to high pressure are 3*T*, whereas those unrelated to high pressure are $2M_1$.

After the pioneering discussion of Sassi et al. (1994) about the crystallographic reasons why pressure favors the 3*T* stacking, numerous new crystal-structure data have appeared indicating that high pressure favors cation ordering and stabilizes the 3*T* polytype over the $2M_1$ one (Pavese et al. 2003), consistent with the elastic properties of the two polytypes (e.g., Curetti et al. 2006). However, the debate is still ongoing. On the one hand, data on natural occurrences of $2M_1$-phengites unrelated to high-pressure metamorphism are few; on the other hand, in their study of a synthetic Mg-rich phengite, Smyth et al. (2000) obtained an equal distribution of 3*T* and $2M_1$ crystals, so that they were compelled to conclude that "there is likely to be little if any pressure effect on polytype distribution" (Smyth et al. 2000 p. 963).

AXANES

The polarization dependence of the mica XANES spectra has been extensively documented before at various *K*-edges (e.g., Al, Fe, and Si: cf. Mottana et al. 2002, Figs. 7–12 therein). This evidence explains clearly the reasons beyond our mistrust for visually interpreting (viz. assessing) experimental data recorded on such platy materials even after careful conventional reduction (Mottana 2004), and justifies our decision to fit them according to the AXANES mathematical procedure (Brouder 1990). It is quite evident that a XANES spectrum taken at any random angle may be far from being representative of the true absorption factor pattern of the mica sample; as a matter of fact, the edge crest intensity may change dramatically, even inverting on rotation, and new features may show up viz. disappear that would change the absorption threshold energy (E_0). Such changes do not develop gradually or, if they do, they are not detected until a significant rotation (ca. 30–40°) has been applied. Indeed, this may be one of the reasons (together with a set-up geometry optimized to record XANES spectra in the fluorescence mode) why the best experimental spectra are almost invariably taken with the sample surface skew with respect to the SR beam-incidence direction.

The AXANES method, as reworked by Brouder (1990) on the basis of the pioneering works by Izraileva (1966, 1969), rationalizes the problem of displaying a spectrum by standardizing it to two positions at fixed sample angles (generally θ = 0

and 90°) with respect to the impinging direction of the linearly polarized horizontal SR beam. Consequently, intensity features determined at such fixed angles become consistent and can be compared among samples differing in composition.

The AXANES method has its theoretical basis on the dipole absorption cross section (σ^D) general approximation. It starts first by demonstrating that its energy dependence is valid over the entire energy range that can be investigated by XAFS (i.e., XANES + EXAFS):

$$\sigma^D(\varepsilon) = \sigma^D(0,0) - \sqrt{8\pi/5} \sum_m Y_2^{m*}(\varepsilon)\, \sigma^D(2,m) \quad (1)$$

where $\sigma^D(\varepsilon) = \sigma^D(0,0)$ for an isotropic (cubic) material as well as for a random powder and $\sqrt{8\pi/5} \sum_m Y_2^{m*}(\varepsilon)$ (with m ranging from –2 to 2) are the spherical harmonics arising from angular contributions depending on rotations about the horizontal θ and vertical ψ axes. The $\sigma^D(2,m)$ coefficient is responsible for the tensor components that affect anisotropic structures.

Given the platy morphology and layered structure of the micas, Cibin et al. (2006) simplified the general formula to only the horizontal angle (θ) that the crystal plane forms with the impinging SR beam polarization direction, thus assuming dichroism, which in fact is valid for dimetric structures or for any structure developed on two dimensions, provided they have a ≥3 rotation symmetry:

$$\sigma^D(\varepsilon) = \sigma^D(0,0) - (1/\sqrt{2})\,(3\cos^2\theta - 1)\,\sigma^D(2,0). \quad (2)$$

Cibin et al. (2006) went farther by re-writing formula 2 for two components, respectively parallel (in-plane, $\sigma_{\|}$) and orthogonal (out-of-plane, $\sigma_{\perp}$) to the reference atomic plane, which in our case is the mica (001) cleavage plane:

$$\sigma_D(\varepsilon) = \sigma_{\|} \sin^2\theta + \sigma_{\perp} \cos^2\theta. \quad (3)$$

Consequently, we can extract the out-of-plane ($\sigma_{\perp}$) and in-plane ($\sigma_{\|}$) component patterns from our experimental XANES spectra, using a simple algorithm that first fits the angle dependence for every experimental point on the basis of formula 2 on all the recorded spectra, then it extrapolates the absorption coefficient to any possible rotation angle, in particular to $\theta = 90°$ ($\sigma_{\perp}$) and $\theta = 0°$ ($\sigma_{\|}$), thus producing the two standard patterns. A computer code based on the same algorithm can then compute back the spectra for any rotation angle, allowing for checking against the recorded experimental spectra for consistency.

Note that at energies where $\sigma^D(2,0) = 0$, the spectrum turns out to be independent on the beam polarization direction. This is the theoretical basis of the "magic angle" theorem developed by Pettifer et al. (1990), which makes it possible to set up the standard sample-holder for powders at an angle ($\theta_m = 35°26$ i.e., $\sin^2\theta_m = 1/3$), where the experimental spectra become isotropic and truly representative, irrespective of whether these are being random or well oriented (cf. Manceau et al. 1998, p. 350). Our algorithm easily calculates such a spectrum at θ_m, and a comparison with experimental spectra recorded around that value can be made, thus allowing checking the calculated results obtained on mica single crystals to be checked against those recorded experimentally on the corresponding powders.

Al *K*-AXANES spectra

Figure 2 demonstrates the results of such a calculation for θ_m in all our phengites. When compared to the experimental Al-XANES spectra, taken on fine disordered powders of end-member synthetic micas containing Al in two coordinations (Mottana et al. 1997b, Fig. 4 therein), our micas indeed show greatest similarity with the muscovite spectrum, but with several fine differences that clearly depend upon their being phengites with compositions departing from the ideal muscovite one. The stacking sequence, apparently, plays a very minor role in this matter, as the synthetic muscovite used at that time was a two-layer disordered monoclinic type i.e., $2M_d$.

All $2M_1$-phengites show three major absorption features in the full multiple scattering (FMS: Natoli and Benfatto 1986) energy range (A at 1561.0, A' at 1563.0, B at 1565.7 eV: notation after Mottana et al. 1997b), followed by a shoulder B' at 1569–1570 eV and by a hump C at ca. 1580 eV i.e., in the intermediate multiple-scattering (IMS: Natoli and Benfatto 1986) energy range. Following the interpretation of Mottana et al. (1997b), recently supported by the calculations of Wu et al. (2003) by the CONTINUUM code (Natoli et al. 2003), we assign feature A to tetrahedral Al, and features A' and B to Al located in the octahedral sheet. The hump C probably refers to ^{VI}Al and marks its interactions with other M cations. Similarly, the weak B' feature is possibly due to interactions between Al and Si in the T sheet.

The θ_m Al-AXANES spectrum of DM 3*T*-phengite can also be interpreted along these lines, actually giving further support to our interpretation. Indeed, feature A is strongly reduced in intensity—it is just a shoulder on the rising limb of feature A'—in agreement with the reduced ^{IV}Al content (0.42 apfu) of the DM mica (Table 1), which is significantly less than in the $2M_1$-ones ($0.68 < {}^{IV}Al < 0.82$ apfu). Furthermore, the threshold energy E_0 of the entire 3*T* spectrum shifts to a higher value by 0.6–0.8 eV with respect to the $2M_1$ ones, as all FMS features do, but in increasing amounts: A' by 0.3 eV and B by 0.8 eV. Moreover, two weak and broad IMS features (C and D) show up, and are resolved enough, D being the strongest and at higher energy (ca. 1584 eV). All these energy changes in our 3*T*-phengite features suggest degrees of interaction along its T and O sheets that are less than those in $2M_1$-phengites.

When comparing the general $2M_1$-phengite spectrum with the 3*T* one, we note two major differences that must be clarified. (1) The main feature in the IMS subregion of the latter sample is shifted significantly to higher energy when compared to the those of the $2M_1$ samples, this positive shift implying a diminution in the unit-cell size of the 3*T* mica (Bianconi et al. 1983; Natoli et al. 1984). Indeed, this is consistent with the overall unit-cell volume contraction (ca. 10%, referred to the 1*M* layer: cf. Curetti et al. 2006), which the DM phengite undergoes as a result of its packed structure and composition, to be related in turn to its ultrahigh-pressure conditions of formation (Sassi et al. 1994, p. 156). (2) Feature A not only is much better defined in $2M_1$-phengites than it is in the 3*T* one, but it also varies in intensity and resolution. Probably, this feature results from hybridization of Al outer electrons with those of other elements in the same structure.

To test these assignments and verify our suggestions, which

would make the characteristics of certain Al-XANES features of phengites to be markers of both their compositions and degrees of order, we are going to use a model that relates the intensity values of their AXANES spectra with the site occupancies determined by EMPA (Table 1). The overall intensity of the ^{IV}Al features (A) at 1561 eV regularly scales down with decreasing ^{IV}Al content, while concurrently, in $2M_1$-phengites, their resolution increases with the Fe content. In particular, we note that there is a relationship between resolution and total Fe content (0.188 vs. 0.322 apfu) for micas AN5 and AC6 (cf. Fig. 2). This finding confirms the significant hybridization effect that an atom rich in weakly bonded external electrons, such as Fe, has on another atom, such as Al, to which it should theoretically be unrelated, but its density of states (DOS) is inevitably affected by the proximity of Fe (cf. Wu et al. 1996). Thus, the scaling trend in intensity confirms that feature D is mostly contributed by ^{IV}Al and has nothing to do with feature C, which is mostly contributed by ^{VI}Al. In further agreement with this conclusion, features A' and B scale opposite to A, and mirror the mica ^{VI}Al contents without any change in their resolution. The peculiar spectrum of the AN5 mica is noteworthy: it exhibits a much stronger B' feature than all other $2M_1$-phengites together with a weak, poorly resolved A' feature. Moreover, this XANES spectrum is the least noisy and best featured of all mica spectra; indeed, it is tempting to interpret this as an indication for a better ordering in both the O and T sheets.

Note that the Al-XANES spectrum of RA1, the Antarctic muscovite, although recorded on a single blade with a different detection method, is practically identical to the $2M_1$-phengite ones. This result agrees well with both its composition and stacking symmetry and supports the correctness of our experimental set-up.

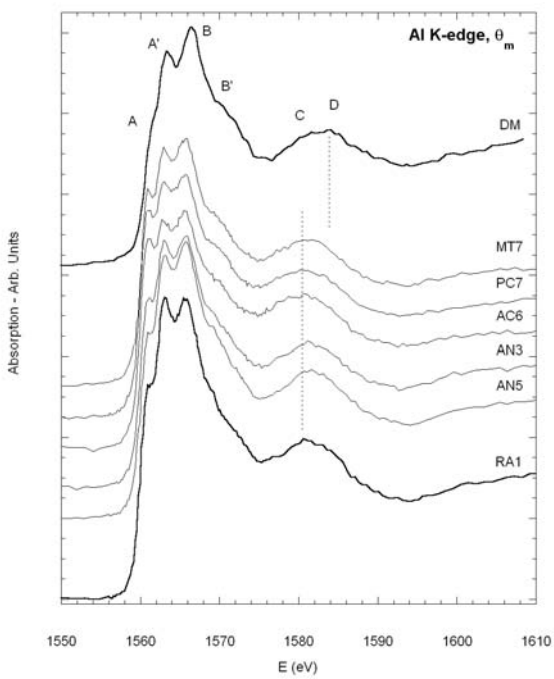

FIGURE 2. Al-AXANES spectra of the studied white micas back-calculated to $\theta_m = 35°26$, the "magic angle" setting (feature labeling after Mottana et al. 1997b, Fig. 4 therein). Key for labels on top of Table 1.

Fe *K*-AXANES spectra

Figure 3 shows the mica patterns extrapolated to $\theta = 0°$, i.e., for $\sigma_{||}$. As demonstrated elsewhere (Cibin et al. 2006), the $\sigma_{||}$ pattern provides the best information on the in-plane distribution of the probed atom and on its relationships with the neighboring atoms; thus, in the present spectra, it reveals the location of Fe and ordering in the O sheet. The $\sigma_{||}$ patterns are simple and feature-poor: they exhibit a weak pre-edge (PE) and three major features (A, B, C) all located in the FMS subregion, which extends from 7116 to 7155 eV. However, the $2M_1$ and $3T$ patterns vastly differ widely in shape, energy, and intensity. Fine differences are also seen among the various $2M_1$-mica patterns as for the intensities of the A and C features relative to edge crest B.

The Fe-AXANES patterns extrapolated to $\theta = 90°$, i.e., for $\sigma_{\perp}$ (Fig. 4), are essentially identical in shape to those extrapolated to $\theta = 0°$, but for the general drop in the feature intensities (ca. –10% rel.). Here, however, the $2M_1$-phengite AXANES patterns exhibit a slightly more articulated sequence of features than the $3T$ one, since there is a discernible shoulder at ca. 7121.5 eV on the rising limb of feature A, probably reflecting the hybridization effect already noted in the Al-AXANES pattern (Fig. 2). The $2M_1$-phengite $\sigma_{\perp}$ patterns agree perfectly in shape with that of the Antarctic muscovite, but differ for energy, as the last one displays a small, but increasingly positive shift (+1.5 eV). The $3T$ $\sigma_{\perp}$ pattern is completely different and mirrors almost perfectly the $\sigma_{||}$ pattern extrapolated for the same mica, as it always consists of one only major edge crest at 7127.1 eV. The reasons behind such an unexpected finding will be discussed later.

Pre-edges in Fe *K*-AXANES spectra

Peaks before the onset of the edge jump (pre-edges) occur in XAFS spectra of most if not all transitional atoms (Mottana 2004). Their location and intensity have been shown to be reliable indicators of the atom oxidation rate and coordination and, in particular, quantitative fitting of PE has become a widespread method together with Mössbauer spectroscopy and ELNES to determine the $Fe^{3+}/\Sigma Fe$ ratio even on mineral grains within thin sections (Dyar et al. 2002a, 2002b).

The very weak PE regions of our $2M_1$-white micas, either as experimentally recorded or as extrapolated from the in-plane and out-of-plane patterns (Fig. 5), never give an indication for $^{IV}Fe^{3+}$ i.e., for the presence of a tetra-ferri-component in phengites (cf. Dyar et al. 2001). This component can be definitively dismissed, leaving only Si and Al to compete for the tetrahedral sites. As a matter of fact, in contrast to the strong PE peaks recorded for Fe when located in an acentric site (Waychunas and Rossman 1983; cf. Dräger et al. 1988; Westre et al. 1997; and particularly Heumann et al. 1997 for theoretical appraisals), all PE regions of our $2M_1$-white micas are flat and show a gradual increase of the background ending up in a shallow bulge just before the onset of the edge jump. This shallow PE profile has been shown to be typical of Fe in octahedral coordination (Waychunas et al. 1983). Only after careful deconvolution can a broad feature having a centroid at 7113.2 ± 0.3 eV and with 0.069–0.077 integrated normalized absorbance be discerned (Fig. 5); moreover, occa-

sionally, there is a hint for another, much weaker feature at lower energy that is not even suitable for fitting. Such a PE profile is common to both the 0 and 90° extrapolated AXANES patterns, although differences in energy and intensity can be observed, which confirm the anisotropic, angle-dependent behavior of the mica structure for the O sheet.

The RA1 muscovite PE (Fig. 5, bottom) shows a single 7113.4 eV peak, having an integrated intensity of 0.083 in the 0° in-plane pattern, and again a single peak but with a centroid at 7113.9 eV and 0.090 integrated intensity in the 90° out-of-plane one; thus, this mica exhibits a greater PE angle-dependency than all other $2M_1$ micas.

By contrast, for the DM $3T$ phengite the PE deconvolution reveals a single weak peak having a centroid at ca. 7112.2 eV and with an integrated intensity 0.046. This peak is the same in both extrapolated spectra, therefore it is plotted only once in Figure 5 (top) as it appears to be totally unaffected by rotation.

Recent work (Petit et al. 2001; Wilke et al. 2001; cf. Galoisy et al. 2001) suggests the PE energy value 7113.5 eV typical for Fe^{3+}, whereas a value 7112.1 eV would be typical for Fe^{2+}. Coordination was shown not to affect the PE energy values, but it would enhance their intensities by as much a three times on going from six- to fourfold coordination (Wilke et al. 2001 Fig. 4). Such XANES results were validated using resonant X-ray emission spectroscopy (RXES: Rueff et al. 2004), a method with greater resolving capacities, and is now understood to be the choice method for characterizing the electronic properties of Fe and other transition metal atoms in complex systems.

Direct comparison with the oriented Fe-XANES spectra experimentally recorded on di- and tri-octahedral micas by Dyar et al. (2001, 2002a, 2002b) confirms that our phengites contain Fe^{3+}

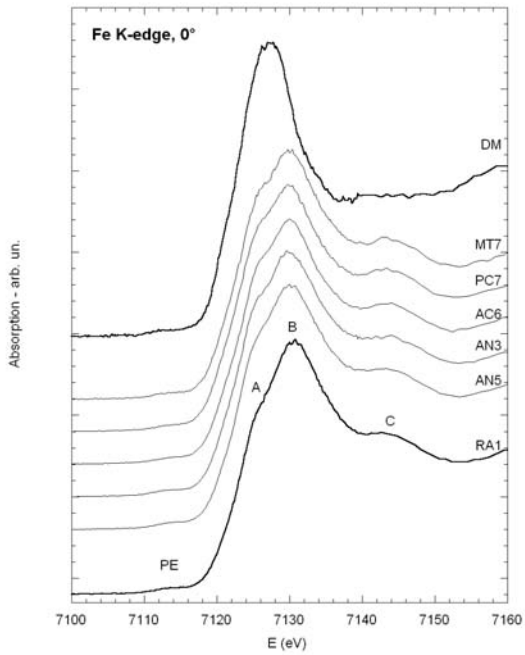

FIGURE 3. Fe-AXANES spectra of the studied white micas extrapolated to θ = 0°, the "in-plane" ($\sigma_{\parallel}$) setting. Key for labels on top of Table 1.

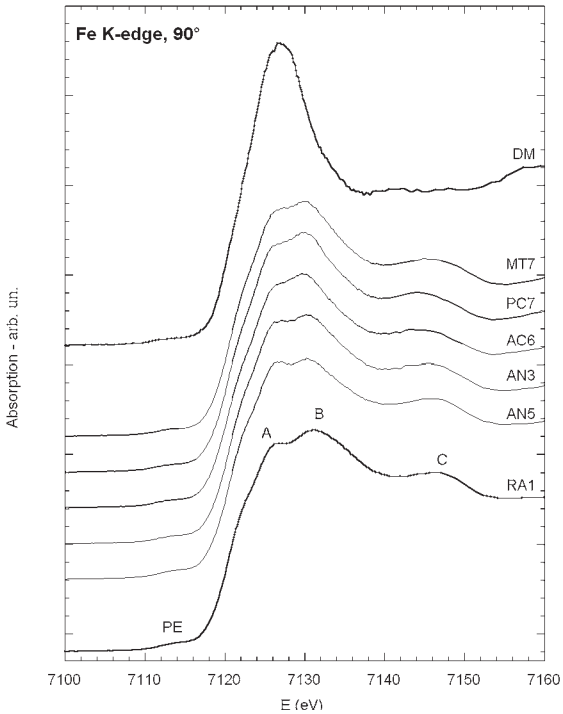

FIGURE 4. Fe-AXANES spectra of the studied white micas extrapolated to θ = 90°, the "out-of-plane" ($\sigma_{\perp}$) setting. Key for labels on top of Table 1.

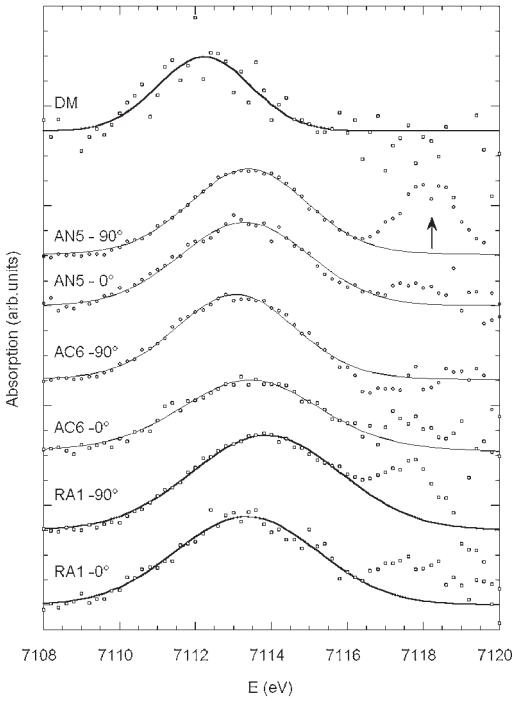

FIGURE 5. Normalized Fe pre-edge regions extracted from the in-plane and out-of-plane AXANES patterns of the $2M_1$- and $3T$-white micas showing extreme Fe contents. The arrow marks the contribution to absorption attributed to hybridization of $^{VI}Fe^{3+}$ with other cations in the octahedral sheet. See text for explanations.

almost to the exclusion of Fe^{2+}. As a matter of fact, if any Fe^{2+} is present, it would only show up as an unresolved contribution in a combination peak shifting the Fe^{3+} peak to lower energy, while scaling it further down to lower intensity (cf. Berry et al. 2003, their Fig. 8). This is indeed the case with our mica AN3 (not shown), the centroid of which is shifted to 7112.8 eV and the total integrated absorbance is down to 0.045. This is also the case with the PE fitting of mica AN6 in the out-of-plane (90°) extrapolated setting (7113.0 eV: Fig. 5): it suggests an anisotropic distribution for Fe within the O sheet, with some more Fe^{2+} located in the direction orthogonal to the sheet.

In conclusion, PE deconvolution show that Fe^{3+} in all $2M_1$-micas is located in regular octahedra, essentially undistorted from centrosymmetric symmetry (Waychunas et al. 1983), but oriented differently so as to undergo small energy shifts that are recorded by the in-plane and out-of-plane AXANES spectra. Furthermore, it hints at the presence of some anisotropically distributed Fe^{2+}, although so little that it is not possible to quantify.

Our PE deconvolution sorted out another intriguing, not yet properly clarified feature. Such an additional feature shows up at slightly higher energy (ca. 7118 eV: Fig. 5, arrow), and it shows up on the rising limb of the $2M_1$-phengite *K*-edges. Its presence cannot be related to either the absorption jump or to other *K*-edge transitions; we interpret it as result of Fe hybridization with other cations located in a similar environment of the mica structure, namely in the O sheet. This contribution is anisotropic and polarization-dependent, since it is consistently more intense in the out-of-plane patterns than in the in-plane ones.

The presence of substantial Fe^{3+} in white mica (up to 90% of total Fe) has been reported several times previously on the basis of Mössbauer evidence (Dyar et al. 1993, 2002a, 2002b; Guidotti et al. 1994). XANES results (even when obtained in critical conditions such as by micro-XANES, SmX) always showed Fe^{3+} values that are in excellent agreement with the Mössbauer data obtained on mica separates from the same rocks, but with a tendency to exceed them by ca. 10% (Dyar et al. 2002c). In our case, the Fe^{2+} content, if any, is minor, but it may be the reason for the unusual hybridization peak detected in all $2M_1$ samples, as already noted elsewhere for garnets (Wu et al. 1996). Note, however, that no Fe^{3+} had been detected by semi-micro chemical methods in the Antarctic muscovite, nor was the presence of Fe^{3+} necessary to account for the small charge deficiency due to the measured low electron density in the M2 site detected during its SC-XRD refinement (Brigatti et al. 1998). Similarly, while solving the structure of their DM 3*T*-phengite, Amisano-Canesi et al. (1994, p. 494) had even found a negative charge deficiency for the M2 site, which they compensated by putting all the available Mg in that site and by filling the M3 site entirely with Al.

The strong similarity between the Fe-AXANES in-plane and out-of-plane patterns observed for most $2M_1$-phengite micas implies that Fe^{3+} distribution and order are essentially, but not entirely, the same both along and across the O plane. The reduced intensity of all the out-of-plane patterns suggests that Fe absorbs less in the latter setting than in the former one, possibly because there is a greater number of collinear Fe atoms that are involved in the photoelectron multiple scattering pathways. Moreover, the well-organized and consistent shape of all patterns suggests that a similarly octahedral distribution exists in all $2M_1$-phengites, irrespectively on their Fe total contents.

We are aware that our finding that Fe^{3+} is dominant in phengites is not welcome news to those who make use of the Mg-ΣFe exchange assuming that all Fe is Fe^{2+}. Therefore, we will try giving further support to our explanation of the present Fe-XAFS results using our EMPA results themselves (Table 1). This type of reasoning already proved to be effective in the Al-XANES case and may support our contention in this one.

Heavy atom substitutions [defined as $(Fe^{2+} + Fe^{3+} + Mg^{2+} + Ti^{4+} + Mn^{2+})/(Fe^{2+} + Fe^{3+} + Mg^{2+} + Ti^{4+} + Mn^{2+} + {}^{VI}Al^{3+})$: Brigatti et al. 1998, p. 777] are limited (0.14–0.23 apfu) in all our $2M_1$-phengites and are not much greater than that determined in the Antarctic muscovite (0.09). Therefore, the conclusions drawn from this mica by single-crystal XRF refinement (Brigatti et al. 1998) can be taken as a model and tested for coherency against our Fe-AXANES data. The Antarctica muscovite has the octahedral *trans*-M1 site vacant, as indeed all dioctahedral micas should, and the *cis*-M2 site is less distorted than ideal muscovite because octahedral substitution increases the <M2-O> distance; indeed, the greater the amount of large cations substituting for Al in the O sheet, the smaller is its distortion (Brigatti et al. 1998, p. 783). This single-crystal XRD result agrees well with our XAFS findings: indeed, our AXANES patterns for Fe, the atom that consistently represents the largest fraction of the cations substituting for Al (in $2M_1$-phengites 55–78%, and in $2M_1$-muscovite 61%), indicate a regular periodic distribution of Fe within the O sheet. It is tempting to try assigning the two features A and B on the edge crest to one or the other of the two *cis*-M2 sites, but there are no clues about it, except that their different intensities may imply different occupancies. Another point for which a satisfactory explanation cannot be found is the observed increasing positive energy shift shown by the muscovite Fe-AXANES patterns with respect to the phengite ones. Such evidence certainly points to some difference in the multiple scattering pathways followed by the photoelectron ejected by Fe along and across the O sheet (Natoli et al. 2003), but it cannot be explained on the basis of the compositional difference.

Compositional difference, although very large (octahedral substitution 0.31, with only 1% due to Fe), cannot explain the strange Fe-AXANES patterns extrapolated for the DM 3*T*-phengite, which is identical for both $\sigma_{\parallel}$ and $\sigma_{\perp}$ i.e., not angle-dependent (Figs. 3 and 4). The Fe *K*-edge signal consists of a unique, broad and intense feature centered at 7127.1 ± 0.2 eV, and the very weak PE bulge at 7112.0 eV (Fig. 5) reveals a small amount of divalent Fe located in an undistorted site that is octahedral or even higher in coordination (cf. Wilke et al. 2001, their Fig. 6). The entire spectra are exceedingly feature-poor and even the rare, broad and very weak oscillations in the EXAFS region (Fig. 6) appear to be rotation-independent. It is tempting to infer from such patterns that the Fe^{2+} we determined in our 3*T*-phengite flake has a completely disordered distribution, much as in a glass (cf. Berry et al. 2003), and is located in a site with a high coordination number.

However, it is very unlikely that glass is present as an inclusion in the 3*T*-white mica from a metagranitoid, viz. white schist equilibrated under ultrahigh-pressure conditions. Indeed, HRTEM and AEM studies on the DM mica showed that it contains oriented platelets (exsolutions) due to pressure release,

but they consist of quartz and talc (Ferraris et al. 2000, 2005). Nevertheless, we cannot rule out a priori another possibility: that the sample we examined contains tiny inclusions of garnet, as this mineral is certainly present in the assemblage (Table 1). The garnet in the Dora Maira white schists is almost pure pyrope (max. 0.91 wt% FeO, corresponding to $X_{prp} \approx 98$; Chopin 1984; Schertl et al. 1991, 1996; Hermann 2003), the Fe-XANES of which we determined in the past (Mottana et al. 1997a) concurrently with a study of Mg-XANES in model compounds and minerals (Cibin et al. 2003, their Fig. 2a). The Fe-XANES pattern for a garnet is compared with the Fe-AXANES of the Dora Maira 3*T*- and AN5 Anterselva 2M_1-phengites (Fig. 6), the latter taken as the representative for the entire Eastern Alps set. The patterns are expanded to contain some initial part of the EXAFS region. Our DM pyrope garnet Fe-XANES spectrum shows a strong, fairly broad edge crest at 7127.1 eV, followed by a week feature at ca. 7140 eV and a more-intense one at ca. 7155 eV. This spectrum compares well with published Fe-XANES spectra of almandine (e.g., Waychunas et al. 1983; Wilke et al. 2001; Dyar et al. 2002b). Furthermore, its deconvoluted PE (Fig. 5, top) looks very much like that fitted on almandine by Wilke et al. (2001, their Fig. 3a), thus confirming Fe to be Fe^{2+} and its distribution over the structure to be isotropic.

The Dora Maira pyrope and 3*T*-phengite Fe-spectra are identical, and both differ from the Anterselva 2M_1-phengite (Fig. 6). In particular, the latter mica shows a significant angle dependence, whereas the DM mica does not (nor does the DM pyrope). Therefore, we conclude that the DM 3*T*-phengite does not contain structural Fe, or, if it does, this cation is very minor indeed; rather, it contains little grains of exsolved pyrope (platelets) that was not detected by P-XRD, EMPA, and PLOM examinations. Indeed, Fe is so scarce in all Dora Maira minerals and over the entire outcrop, as to have suggested a possible meta-evaporitic derivation of the protolith (Schertl et al. 1991, 1996) as an alternative to the more widespread meta-granitic interpretation (Compagnoni and Rolfo 2003; Hermann 2003).

This conclusion brings with itself a question: how much does the presence of pyrope platelets affect the previously studied phengite Al-AXANES spectrum? We believe it does not. Indeed, a simple calculation shows that, assuming that all Fe determined in DM 3*T*-phengite by EMPA (0.12 wt%, Table 1) is located in garnet, the equivalent amount of Al to be attributed to the platelets is only 0.06 wt%. This amount is too small to possibly affect the white mica spectrum or, if it does, only the intensity of the ^{VI}Al edge crest would be affected slightly, leaving the full spectrum (Fig. 2) substantially unchanged. Moreover, even in such an extreme contention that all Fe we recorded in our DM sample is present as garnet inclusions, one experimental evidence is definitively worth pointing out: at 7 KeV energy, XAFS has an extremely high detection capacity and resolving power, as the total Fe in our sample is at the trace level (<100 ppm); consequently, the use of PE fitting for determination of the $Fe^{3+}/\Sigma Fe$ ratio is highly recommended.

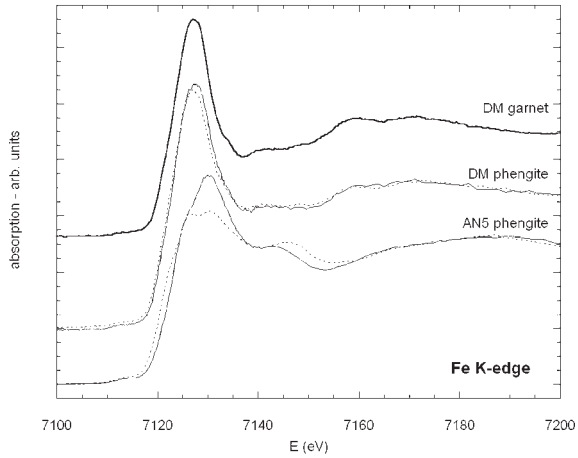

Figure 6. Comparison of the experimental Fe-XANES spectrum of Dora Maira pyrope with the extrapolated Fe-AXANES patterns of Dora Maira 3*T*- and Anterselva 2M_1-white micas. Note the clear dichroic behavior of the in-plane and out-of-plane patterns of the Anterselva 2M_1-phengite as opposed to the isotropic one of the Dora Maira minerals.

Acknowledgments

It is a pleasure for us to contribute to the *American Mineralogist* special issue honoring Charles V. Guidotti, a long-time friend. Charlie was a key person in the painful work of making petrologists aware of the potentials of crystal-chemistry. Ever since his short, but seminal paper about the variation of the white mica d_{002} spacing with metamorphic grade (Guidotti 1966), he was a staunch supporter of the laborious and time-consuming laboratory methods we crystal-chemists deal with in our everyday work. He rapidly realized that EMPA analyses, flowing in a great number to revolutionize the petrologist's work, could not be properly used unless accompanied by appropriate physical measurements. Otherwise, the wealth of chemical data would give the scientist a comfortable, unfortunately often misleading feeling of being able of solving all problems by appropriate handling of the resulting formulae (apfu). By contrast, Charlie stressed the use of sophisticated techniques such as the Mössbauer and XAFS methods, reaching results that would often shock the standard, naïve petrologist, but that did make our understanding of the metamorphic realm really progress.

We dedicate this little contribution to his memory, knowing that his attitude was always to seek for the truth, even when difficult to attain, the more so as, when attained, it was ridden with difficulties to be understood and accepted.

Our research was supported by Ministero dell'Istruzione Università e Ricerca (MIUR) of Italy under project "Effect of petrological variables on mica crystal chemistry" (PRIN 2004). Most XAFS spectra were recorded at Stanford Synchrotron Radiation Laboratory (SSRL), a facility operated by Stanford University and supported by U.S. Department of Energy (DOE), Office of Basic Energy Sciences, and Natural Institute of Health (NIH), Biotechnology Resource Program, Division of Research Resources. We thank the SSRL staff, particularly P. Pianetta, H. Tompkins, and C. Troxel, for advice and technical assistance. Other XAFS spectra were recorded at Laboratori Nazionali di Frascati (LNF), where E. Burattini planned the DAΦNE-Light laboratory and developed the experimental line DXR-1. A. Grilli and A. Raco contributed with their technical skill. At Università Roma, Tre, N. Kreidie and F. de Grisogono assisted in the time-consuming work of converting to AXANES numerous experimental spectra. At Università di Padova, F. Zorzi gave skilful technical assistence in the P-XRD measurements, A. Moretti helped in setting up geothermometers, and T. Cester in optimizing the EMP apparatus for white mica analysis.

References cited

Amisano-Canesi, A., Chiari, G., Ferraris, G., Ivaldi, G., and Soboleva, S.V. (1994) Muscovite- and phengite-3*T*: Crystal structure and conditions of formation. European Journal of Mineralogy, 6, 489–496.

Bailey, S.W. (1984) Appendix. X-ray powder patterns of micas. In S.W. Bailey, Ed., Micas, 13, p. 573–584. Reviews in Mineralogy, Mineralogical Society of America, Chantilly, Virginia.

Beran, A. (2002) Infrared spectroscopy of micas. In A. Mottana, F.P. Sassi, J.B. Thompson Jr., and S. Guggenheim, Eds., Micas: Crystal Chemistry and Metamophic Petrology, 46, p. 351–369. Reviews in Mineralogy and Geochemistry, Mineralogical Society of America, Chantilly, Virginia.

Berry, A.J., O'Neill, H.St.C., Jayasuriya, K.D., Campbell, S.J., and Foran, G.J. (2003) XANES calibrations for the oxidation state of iron in a silcate glass. American Mineralogist, 88, 967–977.

Bianconi, A., Dell'Ariccia, M., Gargano, A., and Natoli, C.R. (1983) Bond length determination using XANES. In A. Bianconi, L. Incoccia, and S. Stipcich, Eds., EXAFS and near edge structure, 27, p. 57–61. Springer Series in Chemical Physics, Springer-Verlag, Berlin.

Bonnin, D., Calas, G., Suquet, H., and Pezerat, H. (1985) Site occupancy of Fe^{3+} in Garfield nontronite: A spectroscopic study. Physics and Chemistry of Minerals, 12, 55−64.

Brigatti, M.F., Frigeri, P., and Poppi, L. (1998) Crystal chemistry of Mg-, Fe-bearing muscovites-$2M_1$. American Mineralogist, 83, 775–785.

Brouder, C. (1990) Angular dependence of X-ray absorption spectra. Journal of Physics: Condensed Matter, 2, 701–738.

Brouder, C., Kappler, J.-P., and Beaurepaire, E. (1990) Theory and application of angle-resolved X-ray absorption spectra. In A. Balerna, E. Bernieri, and S. Mobilio, Eds., 2nd European Conference Programs X-ray Synchrotron Radiation Research Conference Proceedings, 32, 19–22.

Burattini, E., Cinque, G., Dabagov, S., Grilli, A., Marcelli, A., Monti, F., Pace, E., Piccinini, M., and Raco, A. (2004) The DAΦNE-light facility. American Institute of Physics Conference Proceedings, 705, 81–84.

Chopin, C. (1984) Coesite and pure pyrope in high-grade blueschists of the western Alps: a first record and some consequences. Contributions to Mineralogy and Petrology, 86, 107–118.

Cibin, G., Marcelli, A., Mottana, A., Giuli, G., Della Ventura, G., Romano, C., Paris, E., Cardelli, A., and Tombolini, F. (2003) Magnesium X-ray absorption near-edge structure (XANES) spectroscopy on synthetic model compounds and minerals. In A. Bianconi, A. Marcelli, and N.L. Saini, Eds., 19th International Conference on X-ray and Inner-Shell Processes, 32, p. 95–150. Frascati Physics Series, Istituto Nazionale di Fisica Nucleare, Rome.

Cibin, G., Mottana, A., Marcelli, A., and Brigatti, M.F. (2006) Angular dependence of potassium *K*-edge XANES spectra of trioctahedral micas: Significance for the determination of the local structure of the interlayer site. American Mineralogist, 91, 1150–1162.

Compagnoni, R. and Rolfo, F. (2003) UHPM units in the Western Alps. In D.A. Carswell and R. Compagnoni, Eds., Ultrahigh pressure metamorphism, 5, p. 13–49. European Mineralogical Union Notes in Mineralogy, Eötvös University Press, Budapest.

Curetti, N., Levy, D., Pavese, A., and Ivaldi, G. (2006) Elastic properties and stability of coexisting $3T$ and $2M_1$ phengite polytypes. Physics and Chemistry of Minerals, 32, 670–678.

Dräger, G., Frahm, R., Materlik, G., and Brümmer, O. (1988) On the multiplet character of the X-ray transitions in the pre-edge structure of Fe *K* absorption spectra. Physica Status Solidi, B146, 287–293.

Drits, V.A. and Sakharov, B.A. (2004) Potential problems in the interpretation of powder X-ray diffraction patterns from fine-dispersed $2M_1$ and $3T$ dioctahedral micas. European Jounal of Mineralogy, 16, 99–110.

Dyar, M.D. (1993) Mössbauer spectroscopy of tetrahedral Fe^{3+} in trioctahedral micas—Discussion. American Mineralogist, 78, 665–668.

——— (2002) Optical and Mössbauer spectroscopy of iron in micas. In A. Mottana, F.P. Sassi, J.B. Thompson Jr., and S. Guggenheim, Eds., Micas: Crystal Chemistry and Metamophic Petrology, 46, p. 313–369. Reviews in Mineralogy and Geochemistry, Mineralogical Society of America, Chantilly, Virginia.

Dyar, M.D., Delaney, J.S., and Sutton, S.R. (2001) Fe XANES spectra of iron-rich micas. European Journal of Mineralogy, 13, 1079−1098.

Dyar, M.D., Gunter, M.E., Delaney, J.S., Lanzarotti, A., and Sutton, S.R. (2002a) Use of the spindle stage for orientation of single crystals for microXAS: Isotropy and anisotropy in Fe-XANES spectra. American Mineralogist, 87, 1500–1504.

——— (2002b) Systematics in the structure and XANES spectra of pyroxenes, amphiboles, and micas as derived from oriented single crystals. Canadian Mineralogist, 40, 1375–1393.

Dyar, M.D., Lowe, E.W., Guidotti, C.V., and Delaney, J.S. (2002c) Fe^{3+} and Fe^{2+} partitioning among silicates in metapelites: A synchrotron micro-XANES study. American Mineralogist, 87, 514–522.

Ferraris, C., Chopin, C., and Wessicken, R. (2000) Nano- to micro-scale decompression products in ultrahigh-pressure phengite: HRTEM and AEM study, and some petrological implications. American Mineralogist, 85, 1195–1201.

Ferraris, C., Castelli, D., and Lombardo, B. (2005) SEM/TEM-AEM characterization of micro- and nano-scale zonation in phengite from a UHP Dora-Maira marble: Petrologic significance of armoured Si-rich domains. European Journal of Mineralogy, 17, 453–464.

Galoisy, L., Calas, G., and Arrio, M.A. (2001) High-resolution XANES spectra of iron in minerals and glasses: Structural information from the pre-edge region. Chemical Geology, 174, 307–319.

Gebauer, D., Schertl, H.-P., Brix, M., and Schreyer, W. (1997) 35 Ma old ultrahigh-pressure metamorphism and evidence for very rapid exhumation in the Dora Maira Massif, Western Alps. Lithos, 41, 5–24.

Guidotti, C.V. (1966) Variation of the basal spacings of muscovite in sillimanite-bearing pelitic schists of Northwestern Maine. American Mineralogist, 51, 1778–1786.

——— (1984) Micas in metamorphic rocks. In S.W. Bailey, Ed., Micas, 13, 357–467. Reviews in Mineralogy, Mineralogical Society of America, Chantilly, Virginia.

Guidotti, C.V. and Sassi, F.P. (1998a) Petrogenetic significance of Na-K white mica mineralogy: recent advances for metamorphic rocks. European Journal of Mineralogy, 10, 815–854.

——— (1998b) Miscellaneous isomorphous substitutions in Na-K white micas: A review with special emphasis to metamorphic micas. Rendiconti Fisici della Accademia dei Lincei, 9, 57–78.

——— (2002) Constraints on studies of metamorphic K-Na white micas. In A. Mottana, F.P. Sassi, J.B. Thompson Jr., and S. Guggenheim, Eds., Micas: Crystal Chemistry and Metamophic Petrology, 46, p. 413–448. Reviews of Mineralogy and Geochemistry, Mineralogical Society of America, Chantilly, Virginia.

Guidotti, C.V., Yates, M.G., Dyar, M.D., and Taylor, M.E. (1994) Petrogenetic implications of the Fe^{3+} content of muscovite in pelitic schists. American Mineralogist, 79, 793–795.

Güven, N. (1971) The crystal structures of $2M_1$ phengite and $2M_1$ muscovite. Zeitschrift für Kristallographie, 134, 196–212.

Hermann, J. (2003) Experimental evidence for diamond-facies metamorphism in the Dora-Maira massif. Lithos, 70, 163–182.

Heumann, D., Dräger, G., and Bocharov, S. (1997) Angular-dependence in the *K* pre-edge XANES of cubic crystals: The separation of the empty metal e_g and t_{2g} states of NiO and FeO. Journal de Physique IV, 7, Colloque 2 (X-ray Absorption Fine Structure), Supplement du Journal de Physique III d'Avril 1997, Part 1, 481−483.

Ivaldi, G., Ferraris, G., Curetti, N., and Compagnoni, R. (2001) Coexisting $3T$ and $2M_1$ polytypes of phengite from Cima Pal (Val Savenca, western Alps): Chemical and polytypic zoning and structural characterisation. European Journal of Mineralogy, 13, 1025–1034.

Izraileva, L.K. (1966) Theory of the high-energy region of X-ray absorption on monocrystal and polycrystalline materials. Doklady Akademia Nauk SSSR, 11, 777–781 (in Russian).

——— (1969) Polarised and unpolarised X-ray absorption by monocrystals. In X-ray spectra and electronic structure of matter, vol. II, p. 211–221. Instituti Metallofizika Academia Nauk, Kiev (in Russian).

Kisch, H.J., Sassi, R., and Sassi, F.P. (2006) The b_0 lattice parameter and chemistry of phengites from HP/LT metapelites. European Journal of Mineralogy, 18, 207–222.

Kutzler, F.W., Scott, R.A., Berg, J.M., Hodgson, K.O., Doniach, S., Cramer, S.P., and Chang, C.H. (1981) Single-crystal polarized X-ray absorption spectroscopy. Observation and theory for $(MoOS_2)^{2-}$. Journal of the American Chemical Society, 103, 6083–6088.

Lytle, F.W., Greegor, R.B., Sandstrom, D.R., Marques, E.C., Wong, J., Spiro, C.L., Huffman, G.P., and Huggins, F.E. (1984) Measurement of soft X-ray absorption spectra with a fluorescence ion chamber detector. Nuclear and Instrumental Methods in Physics Research, A226, 542–548.

Manceau, A. (1990) Distribution of cations among the octahedra of phyllosilicates: Insight from EXAFS. Canadian Mineralogist, 28, 321–328.

Manceau, A. and Schlegel, M. (2001) Texture effect on polarized EXAFS amplitude. Physics and Chemistry of Minerals, 28, 52–56.

Manceau, A., Bonnin, D., Kaiser, P., and Frétigny, C. (1988) Polarized EXAFS of biotite and chlorite. Physics and Chemistry of Minerals, 16, 180–185.

Manceau, A., Bonnin, D., Stone, W.E.E., and Sanz, J. (1990) Distribution of iron in the octahedral sheet of trioctahedral micas by polarized EXAFS. Comparison with NMR results. Physics and Chemistry of Minerals, 17, 363–370.

Manceau, A., Chateigner, D., and Gates, W.P. (1998) Polarized EXAFS, distance-valence least-squares modeling (DVLS) and quantitative texture analysis approaches to the structural refinement of Garfield nontronite. Physics and Chemistry of Minerals, 25, 347–365.

Manceau, A., Schlegel, M., Chateigner, D., Lanson, B., Bartoli, C., and Gates, W.P. (1999) Application of polarized EXAFS to fine-grained layered minerals. In D. Schulze, P. Bertsch, and J. Stucky, Eds., Synchrotron X-ray Methods in Clay Science, 9, 68–114. Clay Mineral Society Workshop Lectures, Boulder, Colorado.

Manceau, A., Drits, V.A., Lanson, B., Chateigner, D., Wu, J., Huo, D., Gates, W.P., and Stucky, J.W. (2000) Oxidation-reduction mechanism of iron in dioctahedral smectites: II. Crystal chemistry of reduced Garfield nontronite. American Mineralogist, 85, 153–172.

Marcelli, A., Cibin, G., Cinque, G., Mottana, A., and Brigatti, M.F. (2006) Polarized XANES spectroscopy: The *K*-edge of layered K-rich silicates. Radiation Physics and Chemistry, 75, 1596–1607.

Massonne, H.J. (1995) Experimental and petrogenetic study of UHPM. In R.G. Coleman and X. Wang, Eds., Ultrahigh Pressure Metamorphism, p. 33–95. Cambridge University Press, U.K.

Massonne, H.J. and Schreyer, W. (1987) Phengite geobarometry based on the limiting assemblage with K-feldspar, phlogopite, and quartz. Contributions to Mineralogy and Petrology, 96, 212–224.

Mazzoli, C., Meli, S., Peruzzo, L., Sassi, R., and Spiess, R. (2000) Litostratigrafia, magmatismo e metamorfismo nel basamento cristallino delle Alpi Orientali: una rassegna delle attuali conoscenze. Atti e Memorie dell'Accademia Galileiana di Scienze Lettere ed Arti, 117, 25–95.

McConnell, J.D.C., DeVita, A., Kenny, S.D., and Heine, V. (1997) Determination of the origin and magnitude of Al/Si ordering enthalpy in framework aluminosilicates from ab initio calculations. Physics and Chemistry of Minerals,

25, 15–23.
Mookherjee, M., Redfern, S.A.T., and Zhang, M. (2001) Thermal response of structure and hydroxyl ion of phengite-2M_1: An in situ neutron diffraction and FTIR study. European Journal of Mineralogy, 13, 545–555.
Mottana, A. (2004) X-ray absorption spectroscopy in mineralogy: Theory and experiment in the XANES region. In A. Beran and E. Libowitzky, Eds., Spectroscopic methods in mineralogy, 6, 465–552. European Mineralogical Union Notes in Mineralogy, Eötvös University Press, Budapest.
Mottana, A., Della Ventura, G., Romano, C., Marcelli, A., Cibin, G., Paris, E., and Giuli, G. (1997a) A XAS study of pyrope garnets and other minerals. 1997 SSRL Activity Report. Experimental progress report 7-171–7-173.
Mottana, A., Robert, J.-L., Marcelli, A., Giuli, G., Della Ventura, A., Paris, E., and Wu, Z.Y. (1997b) Octahedral versus tetrahedral coordination of Al in synthetic micas determined by XANES. American Mineralalogist, 82, 497–502.
Mottana, A., Marcelli, A., Cibin, G., and Dyar, M.D. (2002) X-ray absorption spectroscopy of the micas. In A. Mottana, F.P. Sassi, J.B. Thompson Jr., and S. Guggenheim, Eds., Micas: Crystal Chemistry and Metamophic Petrology, 46, p. 371–411. Reviews in Mineralogy and Geochemistry, Mineralogical Society of America, Chantilly, Virginia.
Natoli, C.R. (1984) Distance dependence of continuum and bound state of excitonic resonance in X-ray absorption near-edge structure (XANES). In K.O. Hodgson, B. Hedman, and J.S. Penner-Hahn, Eds., EXAFS and near-edge structure III, 38–42.
Natoli, C.R. and Benfatto, M. (1986) A unifying scheme of interpretation of X-ray absorption spectra based on the multiple scattering theory. In P. Lagarde, D. Raoux, and J. Petiau, Eds., EXAFS and Near Edge Structure IV. Journal de Physique 47-C8, 11−23.
Natoli, C.R., Benfatto, M., Della Longa, S., and Hatada, K. (2003) X-ray absorption spectroscopy: State-of-the-art analysis. Journal of Synchrotron Radiation, 10, 26–42.
Nowlan, E.U., Schertl, H.-P., and Schreyer, W. (2000) Garnet-omphacite-phengite thermobarometry of eclogites from the coesite-bearing unit of the southern Dora-Maira Massif, Western Alps. Lithos, 52, 197–214.
Palin, E.J., Dove, M.T., Redfern, S.A.T., Sainz-Díaz, C.I., and Lee, W.T. (2003) Computational study of tetrahedral Al-Si and octahedral Al-Mg ordering in phengite. Physics and Chemistry of Minerals, 30, 293–304.
Pavese, A., Ferraris, G., Prencipe, M., and Ibberson, R. (1997) Cation site ordering in phengite 3T from the Dora-Maira Massif (western Alps): A variable-temperature neutron powder diffraction study. European Journal of Mineralogy, 11, 309–320.
Pavese, A., Ferraris, G., Pischedda, V., and Ibberson, R. (1999a) Tetrahedral order in phengite 2M_1 upon heating, from powder neutron diffraction, and thermodynamic consequences. European Journal of Mineralogy, 11, 309–320.
Pavese, A., Ferraris, G., Pischedda, V., and Mezouar, M. (1999b) Synchrotron powder diffraction study of phengite 3T from the Dora-Maira massif: P-V-T equation of state and petrological consequences. Physics and Chemistry of Minerals, 26, 460–467.
Pavese, A., Ferraris, G., Pischedda, V., and Fauth F. (2001) M1-site occupancy in 3T and 2M_1 phengites by low temperature neutron powder diffraction: Reality or artefact? European Journal of Mineralogy, 13, 1071–1078.
Pavese, A., Curetti, N., Ferraris, G., Ivaldi, G., Russo, U., and Ibberson, R. (2003) Deprotonation and order-disorder reactions as a function of temperature in a phengite 3T (Cima Pal, western Alps) by neutron diffraction and Mössbauer spectroscopy. European Journal of Mineralogy, 15, 357–363.
Petit, P.-E., Farges, F., Wilke, M., and Solé, V.A. (2001) Determination of the iron oxidation state in Earth materials using XANES pre-edge information. Journal of Synchrotron Radiation, 8, 952–954.
Pettifer, R.F., Brouder, C., Benfatto, M., Natoli, C.R., Hermes, C., and Ruiz López, M.F. (1990) Magic-angle theorem in powder X-ray-absorption spectroscopy. Physical Review, B42, 37–42.
Rieder, M., Cavazzini, G., D'yakonov, Y.S., Frank-Kamenetskii, V.A., Gottardi, G., Guggenheim, S., Koval, P.V., Müller, G., Neiva, A.M.R., Radoslovich, E.W., Robert, J.-L., Sassi, F.P., Takeda, H., Weiss, Z., and Wones, D.R. (1998) Nomenclature of the micas. Clays and Clay Minerals, 41, 61–72.
Rimmelé, G., Parra, T., Goffé, B., Oberhänsli, R., Jolivet, L., and Candan, O. (2005) Exhumation paths of high-pressure–low-temperature metamorphic rocks from the Lycian Nappes and the Menderes Massif (SW Turkey): A multi-equilibrium approach. Journal of Petrology, 46, 641–669.
Rowen, M., Rek, Z.U., Wong, J., Tanaka, T., Gorge, G.N., Pickering, I.J., Via, G.H., and Brown, G.E. Jr. (1993) First XAFS spectra with a YB_{66} monochromator. Synchrotron Radiation News, 6, 25–27.
Sanz, J. (1988) Distribution of ions in phyllosilicates by NMR spectroscopy. In A. Mottana and F. Burragato, Eds., Absorption Spectroscopy in Mineralogy, p. 103–144. Elsevier, Amsterdam.
Sassi, F.P., Guidotti, C.V., Rieder, M., and De Pieri, R. (1994) On the occurrence of metamorphic 2M_1 phengites: Some thoughts on polytypism and crystallization conditions of 3T phengites. European Journal of Mineralogy, 6, 151–160.
Sassi, F.P., Cesare, B., Mazzoli, C., Peruzzo, L., Sassi, R., and Spiess, R. (2004) The crystalline basements of the Italian Eastern Alps: A review of the metamorphic features. In D. Castelli and B. Cesare, Eds., Advances in Metamorphic Petrology: Browsing Through Italian Classic Areas, Case Studies, and Approaches. Periodico di Mineralogia, Special Issue 2, 23–42.
Schertl, H.-P. and Schreyer, W. (1996) Mineral inclusions in heavy minerals of the ultrahigh-pressure metamorphic rocks of the Dora Maira Massif and their bearing on the relative timing of the petrological events. In A. Basu and S. Hart, Eds., Reading the isotopic code. Geophysical Monographs, 95, 331–342.
Schertl, H.-P., Schreyer, W., and Chopin, C. (1991) The pyrope-coesite rocks and their country rocks at Parigi, Dora Maira Massif, Western Alps: Detailed petrography, mineral chemistry and PT-path. Contributions to Mineralogy and Petrology, 108, 1–21.
Schmidt, M.W., Dugnani, M., and Artioli, G. (2001) Synthesis and characterization of white micas in the join muscovite-aluminoceladonite. American Mineralogist, 86, 555–565.
Smyth, J.R., Jacobsen, S.D., Swope, R.J., Angel, R.J., Arlt, T., Domanik, K., and Holloway, J.R. (2000) Crystal structures and compressibilities of synthetic 2M_1 and 3T phengite micas. European Journal of Mineralogy, 12, 955–963.
Spear, F.S. (1993) Metamorphic phase equilibria and pressure-temperature-time paths. Mineralogical Society of America Monograph, Chantilly, Virginia.
Spiess, R., Bertolo, B., Borghi, A., and Tinor Centi, M. (2001) Crustal-mantle lithosphere decoupling as a control of the Variscan metamorphism in the Eastern Alps. Australian Journal of Earth Sciences, 48, 479–486.
Tischendorf, G., Rieder, M., Förster, H.-J., Gottesmann, B., and Guidotti, C.V. (2004) A new graphical presentation and subdivision of potassian micas. Mineralogical Magazine, 68, 637–655.
Tombolini, F., Brigatti, M.F., Marcelli, A., Cibin, G., Mottana, A., and Giuli, G. (2002) Local and average Fe distribution in trioctahedral micas: Analysis of the Fe K-edge XANES spectra in the phlogopite-annite and phlogopite-tetra-ferriphlogopite joins on the basis of single-crystal XRD refinements. European Journal of Mineralogy, 14, 1075–1186.
Vieillard, P. (1995) How do uncertainties of the structure refinements influence the accuracy of the prediction of enthalpy of formation? Examples on muscovite and natrolite. Physics and Chemistry of Minerals, 22, 428–436.
Waychunas, G.A. and Rossman, G.R. (1983) Spectroscopic standard for tetrahedrally coordinated ferric iron: $\gamma LiAlO_2$:Fe^{3+}. Physics and Chemistry of Minerals, 9, 212–215.
Waychunas, G.A., Apted, M.J., and Brown, G.E. Jr. (1983) X-ray K-edge absorption spectra of Fe minerals and model compounds: Near-edge structure. Physics and Chemistry of Minerals, 10, 1–9.
Westre, T.E., Kennepohl, P., DeWitt, J.G., Hedman, B., Hodgson, K.O., and Solomon, E.I. (1997) A multiplet analysis of Fe K-edge 1s-3d pre-edge features of iron complexes. Journal of the American Chemical Society, 119, 6297–6314.
Wilke, M., Farges, F., Petit, P.-E., Brown, G.E. Jr., and Martin, F. (2001) Oxidation state and coordination of Fe in minerals: An Fe K-XANES spectroscopic study. American Mineralogist, 86, 714–730.
Wu, Z.Y., Marcelli, A., Mottana, A., Giuli, G., Paris, E., and Seifert, F. (1996) Effects of higher-coordination shells in garnets detected by XAS at the Al K-edge. Physical Review B, 54, 2976–2979.
Wu, Z., Marcelli, A., Cibin, G., Mottana, A., and Della Ventura, G. (2003) Investigation of the mica X-ray absorption near-edge structure spectral features at the Al K-edge. Journal of Physics: Condensed Matter, 15, 7139–7148.

Manuscript received December 29, 2006
Manuscript accepted July 20, 2007
Manuscript handled by Darby Dyar